

An upper limit for current-induced domain wall motion in cylindrical nanowires

Weiwei Wang,^{1,*} Zhaoyang Zhang,¹ Ryan A. Pepper,² Congpu Mu,³ Yan Zhou,⁴ and Hans Fangohr²

¹*Department of Physics, Ningbo University, Ningbo 315211, China*

²*Engineering and the Environment, University of Southampton, SO17 1BJ, Southampton, United Kingdom*

³*School of Science, Yanshan University, Qinhuangdao 066004, China*

⁴*School of Science and Engineering, Chinese University of Hong Kong (Shenzhen), China*

We study the current-driven domain wall motion in cylindrical nanowires using analytical and computational methods. An exact spatiotemporal solution of the Landau-Lifshitz-Gilbert equation including the spin transfer torque terms is reported. The solution allows an arbitrary time-dependent current density. We give an upper velocity limit for the domain wall motion by analyzing the stability of Gaussian wave packets, the limitation indicates that a transverse domain wall can not move arbitrarily fast in cylindrical nanowires although it is free from the Walker limit.

Introduction. The dynamics of magnetic domain walls (DWs) in ferromagnetic nanostrips has drawn considerable attention in the past few years. An effective method to manipulate the DW is with electrical currents [1–7]. The mechanism behind this is the so-called spin transfer torque (STT); when spin-polarized electrons pass through the DW, electrons exert both adiabatic and nonadiabatic torques to the local magnetization [8, 9]. Various complex phenomena make DW motion interesting from a fundamental point of view. For example, in thin nanostrips the Walker breakdown [10] occurs when the speed of a transverse DW reaches a critical velocity due to strong driving forces such as external fields or spin-polarized currents. Hence, the Walker limit is the maximum velocity that a transverse DW can reach in thin strips. Interestingly, a transverse (head-to-head or tail-to-tail) DW does not suffer the Walker limit in cylindrical nanowires [3, 11]; this is because the transverse DW in cylindrical nanowires can rotate freely due to the absence of easy-plane anisotropy. Therefore, we ask if there is a similar physical limit which determines the maximum velocity of the transverse DW in cylindrical nanowires.

To reduce the complexity of the magnetic system, typical methods such as Thiele’s approach [12] and the collective coordinates method [13, 14] have been developed to study the DW dynamics. The key idea is to reduce the degrees of freedom – using fewer parameters to describe the DW dynamics. Alongside these approaches, finding exact solutions, especially time-dependent solution, of the Landau-Lifshitz-Gilbert (LLG) equation plays a special role in understanding fundamental concepts such as DW mass, linear and angular momenta [15]. To date only a few exact spatiotemporal solutions of the LLG equation have been reported in the literature [11, 16]. One example is the well known Walker solution [10], another example describes a moving DW driven by an external field with arbitrary time dependence [11]. In this paper, we will show an exact spatiotemporal solution of the extended LLG equation with spin transfer torque,

and give an upper limit of the maximum velocity for a transverse DW in cylindrical nanowires by analyzing the stability of Gaussian wave packets.

We consider a classical Heisenberg spin chain along the z -direction with energy contributions from exchange interaction and an uniaxial anisotropy [17–20]. The Hamiltonian of the system is

$$\mathcal{H} = -J \sum_i \mathbf{m}_i \cdot \mathbf{m}_{i+1} - D \sum_i (\mathbf{e}_z \cdot \mathbf{m}_i)^2 \quad (1)$$

where \mathbf{m}_i is the unit direction of the i -th magnetic moment $\boldsymbol{\mu}_i$, and $\boldsymbol{\mu}_i = -\hbar\gamma\mathbf{S}_i$ with \mathbf{S}_i being the atomic spin and $\gamma(>0)$ the gyromagnetic ratio. The first term of \mathcal{H} is the ferromagnetic exchange energy ($J > 0$) and the second term represents an uniaxial anisotropy along the z -axis. The dipolar field is approximately included in D as the shape anisotropy for a cylindrical nanowire.

The dynamics of the magnetization in the presence of a spin polarized current is governed by the extended Landau-Lifshitz-Gilbert (LLG) equation with spin transfer torque terms [4, 8, 9]:

$$\begin{aligned} \frac{\partial \mathbf{m}_i}{\partial t} = & -\gamma \mathbf{m}_i \times \mathbf{H}_{\text{eff}} + \alpha \mathbf{m}_i \times \frac{\partial \mathbf{m}_i}{\partial t} + (\mathbf{u} \cdot \nabla) \mathbf{m}_i \\ & - \beta [\mathbf{m}_i \times (\mathbf{u} \cdot \nabla) \mathbf{m}_i] \end{aligned} \quad (2)$$

where $\mathbf{H}_{\text{eff}} = -(1/|\boldsymbol{\mu}_i|)\partial\mathcal{H}/\partial\mathbf{m}_i$ is the total effective field and α is the Gilbert damping. The parameter β describes the contribution of non-adiabatic spin-transfer torque. In this study we assume for the adiabatic spin torque $\mathbf{u} = u\mathbf{e}_z$ with a magnitude $u = |\mathbf{u}|$ of

$$u = \frac{g\mu_B P}{2eM_s} j_e \quad (3)$$

where j_e is the current density, g the Landé factor, μ_B is the Bohr magneton, P is the spin polarization rate, $e(>0)$ is the electron charge and $M_s = |\boldsymbol{\mu}_i|/a^3$ is the saturation magnetization where a is the lattice constant.

An exact spatiotemporal solution. In the continuum limit, by using spherical coordinates $\theta = \theta(z)$ and $\phi = \phi(z)$, we write the magnetization unit vector \mathbf{m} as $\mathbf{m} = (\sin\theta \cos\phi, \sin\theta \sin\phi, \cos\theta)$. The LLG equation (2) can

* wangweiwei1@nbu.edu.cn

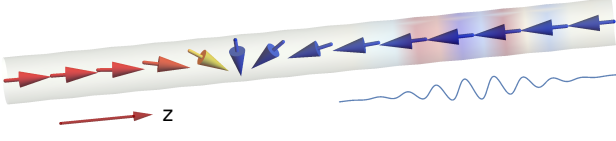


FIG. 1. Schematic illustration of a transverse (head-to-head) DW in a cylindrical nanowire. A Gaussian wave packet will be generated when the charge current is applied suddenly.

be rewritten as

$$\begin{aligned}\dot{\theta} + \alpha \sin \theta \dot{\phi} &= \gamma H_\phi + u \theta' - u \beta \sin \theta \phi', \\ \alpha \dot{\theta} - \sin \theta \dot{\phi} &= \gamma H_\theta + u \beta \theta' - u \sin \theta \phi'.\end{aligned}\quad (4)$$

where we have used the identities $\partial_z \mathbf{m} = \theta' \mathbf{e}_\theta + \sin \theta \phi' \mathbf{e}_\phi$ and $\mathbf{m} \times (\partial_z \mathbf{m}) = \theta' \mathbf{e}_\phi - \sin \theta \phi' \mathbf{e}_\theta$. The overdot in Eq. (4) represents $\partial/\partial t$ and the prime denotes $\partial/\partial z$. The effective fields H_θ and H_ϕ are given by [14]

$$H_\theta = -\frac{1}{\mu_0 M_s} \frac{\delta E}{\delta \theta}, \quad H_\phi = -\frac{1}{\mu_0 M_s \sin \theta} \frac{\delta E}{\delta \phi} \quad (5)$$

where E is the total micromagnetic energy. For the 1d system with Hamiltonian (1) we have $E = a^2 \int w dz$ with $w = A_0 (\partial_z \mathbf{m})^2 - K_z m_z$ where $A_0 = J/2a$ is the exchange constant and $K_z = D/a^3$ is the anisotropy strength. In terms of θ and ϕ , the energy density can be expressed as

$$w = \frac{1}{2} \mu_0 M_s \left[A(\theta'^2 + \sin^2 \theta \phi'^2) + K \sin^2 \theta \right] \quad (6)$$

where $A = 2A_0/\mu_0 M_s$ and $K = 2K_z/\mu_0 M_s$. Therefore, the effective fields H_θ and H_ϕ read

$$\begin{aligned}H_\theta &= A\theta'' - \sin \theta \cos \theta (A\phi'^2 + K), \\ H_\phi &= 2A\theta' \phi' \cos \theta + A\phi'' \sin \theta.\end{aligned}\quad (7)$$

We now search for a domain-wall solution with the form [11]

$$\theta_*(z, t) = \theta_0(z - z_*(t)), \quad \phi_*(z, t) = \phi_*(t), \quad (8)$$

where

$$\theta_0(z) = 2 \arctan \exp(-z/\Delta), \quad \Delta = \sqrt{A/K} \quad (9)$$

describes a head-to-head domain wall and Δ is the typical DW width. The center position of the DW is z_* and ϕ_* represents the DW tilt angle. For the classical spin model $\Delta = a\sqrt{J/2D}$. Note that $\theta'_0 = \sin \theta_0/\Delta$, we have $\theta'_* = \theta'_0 = \sin \theta_0/\Delta$, $\dot{\theta}_* = -\dot{z}_* \theta'_0$, and thus we obtain

$$\begin{aligned}-\dot{z}_* + \alpha \Delta \dot{\phi}_* &= u, \\ \alpha \dot{z}_* + \Delta \dot{\phi}_* &= -u\beta.\end{aligned}\quad (10)$$

The final solution is

$$\dot{\phi}_* = \frac{(\alpha - \beta)u(t)}{(1 + \alpha^2)\Delta}, \quad \dot{z}_* = -\frac{(1 + \alpha\beta)u(t)}{1 + \alpha^2} \quad (11)$$

where $\dot{\phi}_*$ is the angular DW velocity and \dot{z}_* is the DW velocity. This solution can be found in the literature [3, 17]. Here we emphasize that equation (11) is an *exact* solution for the extended LLG equation including the STT terms, and the solution allows an arbitrary time-dependence function $u = u(t)$. This is because we have not assumed the strength and time dependence of the charge current u . This solution additionally holds in the presence of bulk Dzyaloshinskii-Moriya Interaction (DMI) and/or external fields.

As can be seen from Eq. (11), an electrical current along $+z$ moves the DW towards the $-z$ direction [3]. Interestingly, both the DW velocity \dot{z}_* and the angular DW velocity $\dot{\phi}_*$ are linearly dependent on $u(t)$. The DW velocity is not related to the DW width Δ and the angular DW velocity is sensitive to the relative value of β and α . For the case of $\alpha = \beta$ a moving DW has a constant tilt angle.

Micromagnetic simulations show that a moving DW in cylindrical nanowires has an almost vanishing mass [3, 21]. Eq. (11) confirms that the mass of the transverse DW is exactly zero for an arbitrary time-dependent function $u(t)$. It seems that there is no limit for the DW velocity since Eq. (11) is an exact solution for an arbitrary time-dependent current. However, nonlinear effects can play an important role – as an example, spin waves may be emitted when a transverse DW travels in a thin strip [19, 22]; In the presence of external field, the transverse DW in a cylindrical wire also can emit spin waves [23]. As Eq. (11) is a solution in the continuum approximation, it is interesting to ask whether the solution is still valid for the discrete spin model. We will explore this topic by using numerical simulations.

Numerical simulations. We perform numerical simulations by solving Eqs. (1-2) directly [24]. We employ an artificial spin lattice in this study: the lattice constant $a = 1$ nm, $J = 2 \times 10^{-20}$ J and $\mu_0 M_s = 1$ T. In the simulation, a moderate anisotropy $D = 0.01J$ is chosen, which gives the DW width $\Delta = 7.07a$. This anisotropy value satisfies $D/J \ll 2/3$ where $2/3$ is the critical value that separates smooth and sharp DW configurations [25]. We apply a smooth time-dependent charge current $u_1(t) = u_0 \sin^2(2\pi f_0 t)$ with $u_0 = 300$ m/s and $f_0 = 0.125$ GHz to the system. We can estimate that $u_0 = 300$ m/s corresponds to a current density $j = 5.885 \times 10^{13}$ A/m² if $P = 0.7$. As a comparison, we also use a square-wave current pulse $u_2(t)$ with amplitude u_0 and period $T = 2$ ns to drive the DW.

The inset of Fig. 2(a) shows the current pulses u_1 and u_2 . The corresponding DW displacements are shown in Fig. 2(a), as we can see, a Gaussian wave packet is generated for the square-wave current pulse u_2 case.

An animation [I.gif] is included in the Supplemental Material [26]. This results indicate that Eq. (11) is approximately valid for the discrete model if the charge current varies smoothly with respect to time. Note that in the micromagnetic model, the Gaussian wave packet is not expected for the u_2 case; the creation of the wave

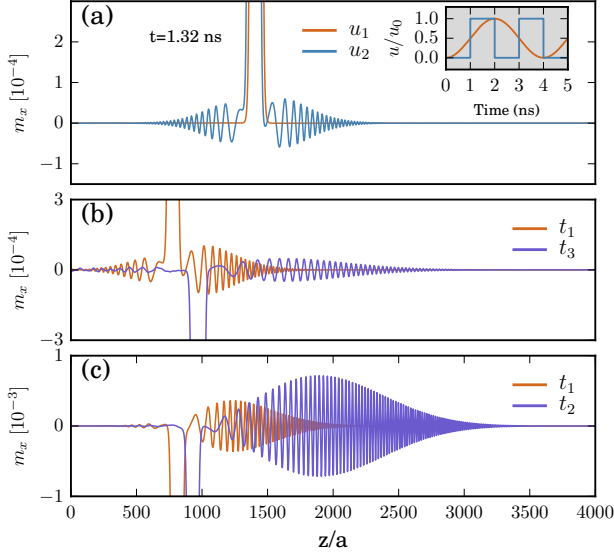


FIG. 2. Numerical simulations for the propagation of the Gaussian wave packets. (a) The x -component magnetization m_x at $t = 1.32$ ns for a sinusoidal pulse u_1 and a rectangular pulse u_2 : a Gaussian wave packet is generated for u_2 case. In the simulation $\alpha = 0.015$ and $\beta = 0.03$ have been used. Inset: Plots of current densities u_1 and u_2 as a function of time. (b) The m_x profiles at $t_1 = 0.32$ ns and $t_3 = 0.8$ ns for a uniform charge current $u = 400$ m/s with $\beta = 0.05$. (c) Same as (b) but $t_2 = 0.56$ ns, $\beta = 0.1$ and $u = 500$ m/s.

packet is a result of the discrete lattice. It is well known that a discrete DW behaves differently to a smooth DW, with peculiar DW motion in the presence of a Peierls potential [27] and in the reflection of spin waves at the wall [25], due to the discretisation.

Beyond the stable motion. The nonadiabatic STT influences the spin waves amplitude significantly, leading to either a weakened or enhanced spin wave attenuation depending on the relative direction between wave vector and \mathbf{u} [23, 28]. Fig. 2(b-c) show the simulation results for the propagation of the Gaussian wave packets driven by uniform currents with different β and different u .

For the scenario that $\beta = 0.05$ and $u = 400$ m/s [Fig. 2(b)] the amplitude of the Gaussian wave decreases, there are two reasons responsible for the amplitude decrease. There are two reasons for this decay: the existence of Gilbert damping and the intrinsic delocalization due to the quadratic dispersion relation of spin waves. However, as shown in Fig. 2(c), the amplitude increases exponentially when $\beta = 0.1$ and $u = 500$ m/s, leading to a magnetization reversal, see video [II.gif] in Supplemental Material [26].

We now investigate the case of a head-to-head DW that separates two domains with magnetization $\mathbf{m} = (0, 0, 1)$ and $\mathbf{m} = (0, 0, -1)$. For the given energy density [Eq. (6)], the corresponding effective field is $\mathbf{H}_{\text{eff}} = A(\partial^2 \mathbf{m} / \partial z^2) + K m_z \mathbf{e}_z$. Substituting the effective field

\mathbf{H}_{eff} into Eq. (2), one obtains

$$\begin{aligned} \frac{\partial \mathbf{m}}{\partial \tau} = & -\mathbf{m} \times \frac{\partial^2 \mathbf{m}}{\partial \xi^2} - m_z \mathbf{m} \times \mathbf{e}_z + \alpha \mathbf{m} \times \frac{\partial \mathbf{m}}{\partial \tau} \\ & + b \frac{\partial \mathbf{m}}{\partial \xi} - \beta b \mathbf{m} \times \frac{\partial \mathbf{m}}{\partial \xi} \end{aligned} \quad (12)$$

where $\tau = \gamma K t$, $\xi = z / \Delta$ and $b = u / (\gamma K \Delta)$. By introducing the complex transformation [29, 30]

$$\psi = m_x - i m_y \quad m_z = \sqrt{1 - |\psi|^2} \quad (13)$$

and linearizing the LLG equation around $\mathbf{m} = (0, 0, 1)$, we arrive at a Schrödinger-type equation

$$i(1 + \alpha i) \frac{\partial \psi}{\partial \tau} = -\frac{\partial^2 \psi}{\partial \xi^2} + \psi + i b(1 + \beta i) \frac{\partial \psi}{\partial \xi} \quad (14)$$

The complex conjugate of this corresponds to the linearized equation around $\mathbf{m} = (0, 0, -1)$ with transformation $m_z = -\sqrt{1 - |\psi|^2}$. A typical solution of Eq. (14) is the travelling wave in the form $e^{i(q\xi - \omega\tau)}$ where ξ and ω are dimensionless wave vector and frequency. However, in the presence of damping (i.e., $\alpha > 0$), a complex frequency $\tilde{\omega}$ or wave vector \tilde{q} must be introduced, which corresponds to a finite linewidth or amplitude decay [28, 31] of spin waves, respectively. For spin waves with localized shape, we chose the former [32], and thus we look for a solution in the form

$$\psi(\xi, \tau) = \frac{\psi_0}{\sqrt{2\pi}} \int_{-\infty}^{\infty} f(q) e^{i(q\xi - \tilde{\omega}\tau)} dq \quad (15)$$

with $f(q) = e^{-a(q-q_0)^2}$ and $|\psi_0| \ll 1$. This solution represents a Gaussian wave packet. Substituting Eq. (15) into Eq. (14), we find

$$\tilde{\omega} = (\omega_r - i\omega_i) / (1 + \alpha^2) \quad (16)$$

where $\omega_r = (1 + q^2 - bq) - \alpha\beta bq$ gives the dispersion rela-

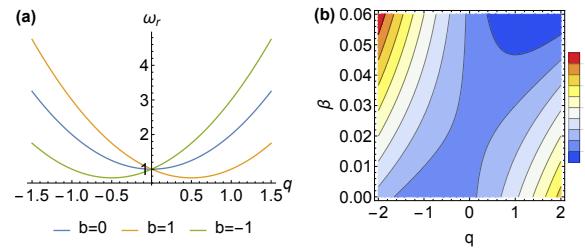


FIG. 3. (a) Dispersion relations for $b = 0$, $b = -1$ and $b = 1$. (b) Contour plot of the dissipation rate ω_i as a function of q and β for $\alpha = 0.02$ and $b = -1.5$.

tion of spin waves and $\omega_i = \alpha(1 + q^2 - bq) + \beta bq$ indicates the energy dissipation during the spin wave propagation. Fig. 3(a) shows the dispersion relations for different values of b . We can see that the wave vector q is shifted

in the presence of spin current, and the spin current is proportional to b . This wave vector shift is similar to case that induced by the DMI [33], resulting in an asymmetric spin-wave dispersion. Note that the spin wave frequency ω_r is negative if $|b + \alpha\beta| > 2$. It is estimated that $b \sim 2$ corresponds to $u = 1250.7$ m/s for the parameters we used above. The domain wall velocity \dot{z}_* can be obtained using eq. (11) and is of similar magnitude.

Fig. 3(b) shows a contour plot of the dissipation rate ω_i as a function of β and q for $\alpha = 0.02$ and $b = -0.15$, it is found that in the top right corner ω_i is negative, which indicates that β term may leads to a negative dissipation rate if $|b| < 2$. For the case that $\alpha = 0$ and $b = 0$, the solution of $\psi(\xi, \tau)$ reduces to

$$\psi(\xi, \tau) = \sqrt{\frac{\psi_0^2/2}{a + i\tau}} e^{i[q_0\xi - (1+q_0^2)\tau] - (\xi - 2q_0\tau)^2/4(a + i\tau)} \quad (17)$$

Eq. (17) describes a moving Gaussian wave packet with group velocity $v_g = (\partial\omega_r/\partial q)|_{q=q_0} = 2q_0$. The packet delocalizes rapidly – its amplitude decreases and width increases with time, similar to the one shown in Fig. 2(b).

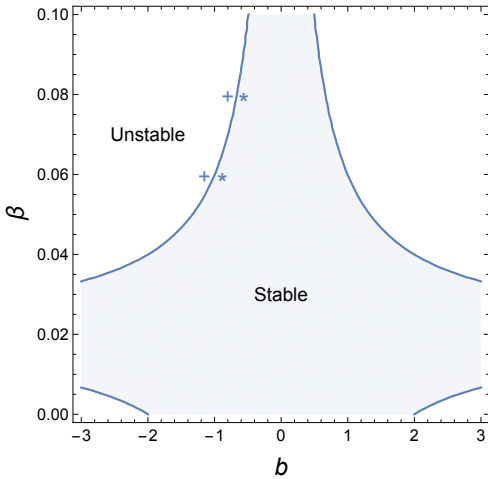


FIG. 4. The critical current density for $\alpha = 0.02$. The plus symbols and stars are numerical simulation results where the plus signs represent the unstable region while the stars denote the stable region.

To analyze the stability of the Gaussian packets, we define the total energy $P(\tau) = (2\pi/\psi_0^2) \int_{-\infty}^{\infty} |\psi(\xi, \tau)|^2 d\xi$. For the case $b > 0$, it is convenient to compute P in q space, i.e., $P = \int_{-\infty}^{\infty} |\tilde{\psi}(q, \tau)|^2 dq$ where $\tilde{\psi}(q, \tau) = f(q)e^{-i\tilde{\omega}\tau}$ since Eq. (15) can be considered as a Fourier transformation of $\tilde{\psi}(q, \tau)$. Hence, we obtain

$$P = \sqrt{\frac{\pi/2}{a + \alpha\tilde{\tau}}} \exp \left[-\frac{g_0\tilde{\tau}^2 + g_1\tilde{\tau}}{2(a + \alpha\tilde{\tau})} \right] \quad (18)$$

where $\tilde{\tau} = \tau/(1 + \alpha^2)$, $g_0 = (\alpha - \beta)^2 b^2 - 4\alpha^2$ and $g_1 = -4a[\alpha q_0^2 + b(\beta - \alpha)q_0 + \alpha]$. It is clear that the sign of g_0 determines the total energy of the Gaussian wave packet over longer time scales; a positive g_0 suppresses the Gaussian wave packet while a negative g_0 leads to a growing wave packet. Therefore, the critical current density is determined by

$$b_c = \frac{2\alpha}{|\alpha - \beta|}, \quad (19)$$

which gives $u_c = 2\gamma\sqrt{AK}\alpha/|\alpha - \beta|$ and thus $j_c^e = 2eM_s u_c/(g\mu_B P)$. It is perhaps surprising that this critical current density is independent from the group velocity q_0 and the Gaussian wave width while for the spin wave case the amplitude decaying length is influenced by the wave vector of spin waves for a given current density. As a comparison, the critical u for Walker breakdown in the presence of easy-plane anisotropy K_{\perp} is approximately established as $u_c^w = (1/4)u_c\kappa/\sqrt{1 + \kappa/2}$ [4] where $\kappa = K_{\perp}/K_z$. For a typical $\kappa = 0.5$ one obtains $u_c^w \approx 0.1u_c$.

Fig. 4 plots the critical current density using blue lines. The corresponding simulation results are also shown in Fig. 4 with plus symbols and stars. The plus signs represent the unstable region while the stars denote a stable motion. When $\alpha = \beta$, the total energy of the Gaussian wave can be simplified to

$$P = \sqrt{\frac{\pi/2}{a + \alpha\tilde{\tau}}} e^{-2\alpha\tilde{\tau} - 2aq_0^2\alpha\tilde{\tau}/(a + \alpha\tilde{\tau})}. \quad (20)$$

We find that P is independent from the charge current b and decreases with $\tilde{\tau}$ for arbitrary q_0 . The reason is that $\omega_i > 0$ even for a negative spin wave frequency ω_r when $\alpha = \beta$. Therefore, the solution (11) is quite stable if $\alpha = \beta$ because the spin wave is suppressed.

Conclusion. In summary, we have studied the current-driven domain wall motion in a cylindrical nanowire. We have presented an exact spatiotemporal solution of the extended LLG equation with spin transfer torque terms. The solution holds for charge currents with an arbitrary time dependence. By analyzing the stability of the Gaussian wave packet, we give an upper velocity limit for the domain wall motion driven with spin currents. The limitation indicates that a transverse domain wall can not move arbitrarily fast in cylindrical nanowires though it is not subject to the Walker limit.

Acknowledgement. We acknowledge the financial support from National Natural Science Foundation of China (Grant No. 11404280) and EPSRC under Centre for Doctoral Training grant EP/L015382/1. This work is sponsored by K.C.Wong Magna Fund in Ningbo University.

-
- [1] L. Berger, Phys. Rev. B **33**, 1572 (1986).
 - [2] S. S. P. Parkin, M. Hayashi, and L. Thomas, Science **320**, 190 (2008).
 - [3] M. Yan, A. Kákay, S. Gliga, and R. Hertel, Phys. Rev. Lett. **104**, 057201 (2010).
 - [4] A. Thiaville, Y. Nakatani, J. Miltat, and Y. Suzuki, Europhys. Lett. **69**, 990 (2005).
 - [5] M. Hayashi, L. Thomas, C. Rettner, R. Moriya, Y. B. Bazaliy, and S. S. P. Parkin, Phys. Rev. Lett. **98**, 037204 (2007).
 - [6] L. Thomas, R. Moriya, C. Rettner, and S. S. P. Parkin, Science **330**, 1810 (2010).
 - [7] M. Franchin, A. Knittel, M. Albert, D. S. Chernyshenko, T. Fischbacher, A. Prabhakar, and H. Fangohr, Phys. Rev. B **84**, 094409 (2011), 1104.3010.
 - [8] S. Zhang and Z. Li, Phys. Rev. Lett. **93**, 127204 (2004).
 - [9] G. Tatara, H. Kohno, and J. Shibata, Phys. Rep. **468**, 213 (2008).
 - [10] N. L. Schryer and L. R. Walker, J. Appl. Phys. **45**, 5406 (1974).
 - [11] A. Goussev, J. M. Robbins, and V. Slastikov, Phys. Rev. Lett. **104**, 147202 (2010).
 - [12] A. Thiele, Phys. Rev. Lett. **30**, 230 (1973).
 - [13] O. A. Tretiakov, D. Clarke, G. W. Chern, Y. B. Bazaliy, and O. Tchernyshyov, Phys. Rev. Lett. **100**, 127204 (2008).
 - [14] B. Hillebrands and A. Thiaville, *Spin Dynamics in Confined Magnetic Structures III* (Springer, New York, 2006).
 - [15] O. Tchernyshyov, Ann. Phys. (N.Y.) **363**, 98 (2015).
 - [16] Z. Z. Sun and X. R. Wang, Phys. Rev. Lett. **97**, 077205 (2006).
 - [17] R. Wieser, E. Y. Vedmedenko, and R. Wiesendanger, Phys. Rev. B **81**, 024405 (2010).
 - [18] R. Wieser, E. Y. Vedmedenko, P. Weinberger, and R. Wiesendanger, Phys. Rev. B **82**, 144430 (2010).
 - [19] X. S. Wang and X. R. Wang, Phys. Rev. B **90**, 184415 (2014).
 - [20] W. Wang, M. Beg, B. Zhang, W. Kuch, and H. Fangohr, Phys. Rev. B **92**, 020403 (2015).
 - [21] R. Hertel and A. Kákay, J. Magn. Magn. Mater. **379**, 45 (2015).
 - [22] B. Hu and X. R. Wang, Phys. Rev. Lett. **111**, 027205 (2013).
 - [23] H. Xia, J. Chen, X. Zeng, and M. Yan, Phys. Rev. B **93**, 140410 (2016).
 - [24] W. Wang, M.-A. B. D. Cortes, M. Vousden, B. Carey, M. Beg, and H. Fangohr, Fidimag, <http://computationalmodelling.github.io/fidimag/>.
 - [25] P. Yan and G. E. W. Bauer, Phys. Rev. Lett. **109**, 087202 (2012).
 - [26] See supplementary material at [URL] for the animations of the creation and propagation of Gaussian wave packets. See the scripts and notebooks at <https://github.com/fangohr/paper-supplement-2016-domain-wall-motion> for the figures and animations in this paper.
 - [27] F. J. Buijnsters, A. Fasolino, and M. I. Katsnelson, Phys. Rev. Lett. **113**, 217202 (2014).
 - [28] S.-M. Seo, K.-J. Lee, H. Yang, and T. Ono, Phys. Rev. Lett. **102**, 147202 (2009).
 - [29] Z. D. Li, Q. Y. Li, L. Li, and W. M. Liu, Phys. Rev. E **76**, 026605 (2007).
 - [30] F. Zhao, Z. D. Li, Q. Y. Li, L. Wen, G. Fu, and W. M. Liu, Ann. Phys. (N.Y.) **327**, 2085 (2012).
 - [31] K. Sekiguchi, K. Yamada, S. M. Seo, K. J. Lee, D. Chiba, K. Kobayashi, and T. Ono, Phys. Rev. Lett. **108**, 017203 (2012).
 - [32] M. Covington, T. M. Crawford, and G. J. Parker, Phys. Rev. Lett. **89**, 237202 (2002).
 - [33] J.-H. H. Moon, S.-M. M. Seo, K.-J. J. Lee, K.-W. W. Kim, J. Ryu, H.-W. W. Lee, R. D. McMichael, and M. D. Stiles, Phys. Rev. B **88**, 184404 (2013).